Jurnal Polimesin
Department of Mechanical Engineering
State Polytechnic of Lhokseumawe
http://e-jurnal.pnl.ac.id/polimesin
e-ISSN : 2549-1999 No. : 1 Month : February
p-ISSN : 1693-5462 Volume : 24 Year : 2026

Processing dates: received on 2026-01-19, reviewed on 2026-02-11, accepted on 2026-02-17 and online availability on 2026-02-28

Displacement and Von Mises stress analysis in hydraulic actuator cylinder materials for military vehicle applications

Massuradi Simbolon[1,2], Asrori[1], Satworo Adiwidodo[1], Sugeng Hadi Susilo[1]
[1]Department of Mechanical Engineering, Malang State Polytechnic, Malang 65141, Indonesia
[2]Department of Combat Vehicle Engineering, Army Polytechnic (Poltekad), Batu 65321, Indonesia
Corresponding author: simbolon071@gmail.com
asrori@polinema.ac.id
satworo.adiwidodo@polinema.ac.id
sugeng.hadi@polinema.ac.id

Abstract

Material selection is crucial for ensuring the structural reliability of hydraulic actuator cylinders operating under high-pressure and dynamic loading conditions. Conventional methods, which focus on cost or manufacturing ease, may neglect detailed performance analysis, leading to local stress concentrations exceeding material strength. This research addresses this issue by comparing the performance of AISI 1020, AISI 1035, and AISI A2 tool steel using Finite Element Analysis (FEA) and conducting experimental testing to assess displacement, Von Mises stress distribution, and safety factor under various loads (450 N, 900 N, and 1350 N). The experimental results show that AISI A2 performed best in structural response with the highest safety margin, AISI 1035 exhibited the highest stress, and AISI 1020 exhibited the highest displacement. In FEA, AISI A2 showed a controlled maximum displacement of 0.28 mm with a safety factor of 3.94, compared with AISI 1020, which reached 0.82 mm and a safety factor of 1.23. The findings support the significant influence of material mechanical properties on actuator structural integrity and confirm that AISI A2 provides the highest resistance to deformation and stress concentration. The study demonstrates the effectiveness of FEA in optimizing actuator material selection for high-load applications.

Keywords:
Finite Element Analysis (FEA), hydraulic actuator, piston cylinder, Von Mises stress, displacement

1 Introduction

The selection of appropriate materials for military vehicle hydraulic actuators must be able to withstand high operational pressures and dynamic loads. Material failure in critical components can cause catastrophic system damage, jeopardizing the operational readiness of military vehicles. Traditional methods of material selection often rely on cost factors or ease of production, without considering detailed performance analysis under varying load conditions. This can cause local stress concentrations to exceed the material's strength limits. In addition, it is very important in military vehicles to maintain structural integrity, reducing the risk of plastic deformation and fatigue failure. Therefore, actuator cylinder designs must meet the necessary safety factors and performance standards. Material performance analysis of military vehicle engine components, especially piston cylinders, is a critical area, particularly in improving operational efficiency and durability under extreme conditions.

Recent research has utilized Finite Element Analysis (FEA) to evaluate the mechanical properties and performance of various materials used in these critical components. Several studies have explored the mechanical behavior of materials such as aluminum alloys, titanium alloys, and steel under stress, thermal load, and cyclic fatigue conditions [1].

Several studies have focused on comparing the performance of these materials in the context of military vehicle engines [2]. This research shows that material selection significantly affects the durability and reliability of engine components. For example, titanium alloys [3] are known for their high strength-to-weight ratio and corrosion resistance, making them ideal for high-performance applications. On the other hand, aluminum alloys [4], known for their lightweight characteristics, provide benefits in reducing the overall weight of military vehicles, although their lower strength limits may require optimization in design. The application of FEA in this context allows for the identification of optimal material selection based on specific performance criteria such as thermal conductivity, tensile strength, and fatigue resistance [5].

In the field of military vehicle engineering, continuous advances in materials technology are improving the material selection process for components that experience high stress [6]. The integration of multi-physics simulations, including heat transfer, fluid dynamics, and material fatigue, has become increasingly popular in recent years [7].

The interaction of various forces acting on piston cylinder designs, these advanced simulation techniques enable more accurate predictions of component behavior under various conditions [8]. These innovations not only contribute to improved material performance but also pave the way for the development of next-generation military vehicles with better efficiency and durability [9].

Despite the increasing use of FEA in evaluating component performance, most previous studies still discuss material capability in a general manner or focus on different material classes (e.g., aluminum or titanium) without providing a direct, quantitative comparison of steels that are commonly applied in actuator cylinders under the same representative service loads. In addition, studies that simultaneously link stress distribution, displacement response, and safety factor with experimental verification for actuator cylinder applications, especially for AISI 1020, AISI 1035, and AISI A2, are still limited. As a result, material selection for military vehicle hydraulic actuator cylinders often relies on practical considerations rather than performance-based evidence under high-pressure loading conditions. Therefore, this study fills the gap by combining FEA and experimental testing at 450 N, 900 N, and 1350 N to compare the structural response of AISI 1020, AISI 1035, and AISI A2 and to determine the most suitable material for reliable actuator cylinder performance.

2 Study literature

2.1 Mechanism modeling

SolidWorks® creates a detailed representation of the mechanism, focusing on targeted and essential parts to ensure operational efficiency. Special attention was given to the rocker arm, a component that experiences significant fatigue loads during operation. To assess its structural integrity and durability, FEA was performed, specifically evaluating linear static and fatigue loads. In addition, this section also discusses the kinematics of the joints and the forces generated by the pneumatic cylinders, which directly affect the performance and responsiveness of the steering mechanism. The dynamic behavior of the linkage is analyzed to achieve a balance between quick response during vehicle operation and the prevention of damage caused by excessive acceleration. The assembly of the mechanism and its key components, as shown in Fig. 1, provides a comprehensive framework for understanding the design. An exploded view of the steering mechanism provides the

components. Description in Fig. 1 are, 1. The inlet port is the port where hydraulic fluid enters the actuator system. This fluid provides pressure to move the piston inside the cylinder; 2. The outlet port is the port used to discharge hydraulic fluid after it has been used by the actuator. The fluid flows out through this port after moving the piston; 3. The piston rod is the part that connects the piston to the outside of the cylinder and converts hydraulic energy into mechanical motion.

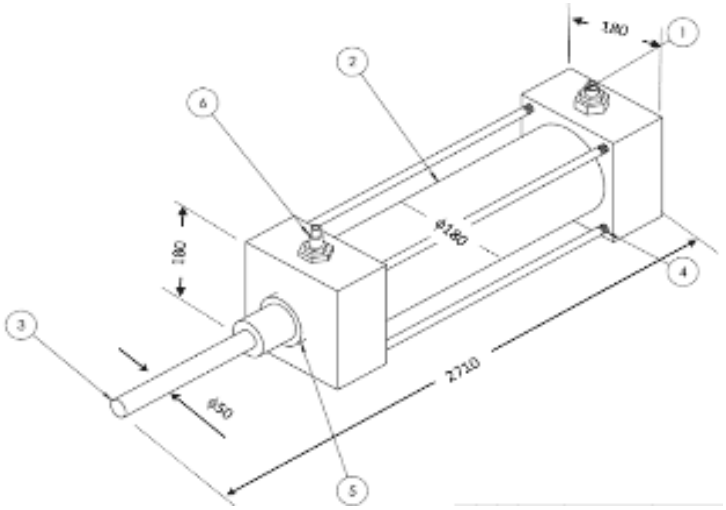

Fig. 1. Position of cylinder and components

This piston rod usually moves back and forth inside the cylinder, depending on the fluid pressure; 4. The cylinder wall is the part of the actuator that withstands hydraulic fluid pressure. It is usually made of a strong material to withstand the forces generated during operation; 5. The piston is the main component in the cylinder that receives pressure from the hydraulic fluid. This piston moves forward or backward, producing the desired mechanical movement; 6. Sealing Caps are components used to close the top and bottom of the cylinder, ensuring that there are no hydraulic fluid leaks. They also serve as connectors to secure other parts and prevent leaks during operation.

2.2 Relationship between pressure and Von Mises stress

This pressure causes hoop stress, radial stress, and axial stress on the tube material. For cylindrical tubes under internal pressure, the Von Mises stress formula can be calculated by considering these stress components [10].

2.2.1 Stresses occurring in cylindrical tubes

In internally pressurized cylindrical tubes, the stresses acting are:

a. Circumferential stress (σθ)

This is the stress acting around the cylindrical wall in a circular direction, which is the greatest stress in the tube, as shown in Eq. (1).

$$\sigma\theta = \frac{pr}{t} \tag{1}$$

where p is the internal pressure (Pa or N/m²), r is the inner radius of the tube (m), and t is the wall thickness of the tube (m).

Eq. (1) expresses the hoop stress that arises on the wall of a thin-walled cylinder due to internal pressure (p), where the fluid pressure acting in all directions produces a force that tends to split the cylinder circumferentially, so that the cylinder wall experiences tensile stress in the circumferential direction that is proportional to the pressure and the radius of the cylinder (r), and inversely proportional to the wall thickness (t). In the context of Von Mises equivalent stress, this hoop stress is the dominant principal stress component, because in thin-walled pressure vessels, there are two principal stresses, namely hoop stress $\sigma\theta$ and tensile stress $\sigma z = \frac{pr}{2t}$. Therefore, when incorporated into the Von Mises criterion for plane stress conditions $\sigma vm = \sqrt{\sigma_\theta^2 - \sigma\theta\sigma z + \sigma_z^2}$, the Von Mises stress value will be greatly influenced by the magnitude of the hoop stress, which explains why plastic failure in pressurized pipes or tubes is generally controlled by hoop stress rather than tensile stress.

b. Radial stress

This stress acts in a radial direction perpendicular to the tube surface and will be smaller than the circumferential stress, as seen in Eq. (2).

$$\sigma r = -\frac{pr^2}{t^2} \tag{2}$$

Eq. (2) expresses the radial stress that arises on the wall of a cylinder or pipe due to internal pressure, where the negative sign indicates that the stress is compressive and its direction is perpendicular to the wall surface, i.e., from the fluid towards the material; physically, this formula describes how internal pressure (p) not only produces tensile stress, but also produces a radial stress component that presses against the wall, with its magnitude increasing quadratically with radius (r) and decreasing sharply with increasing wall thickness (t). so that its effect is relatively small in thin-walled vessels but becomes significant in thicker walls or high stress gradient conditions. In relation to Von Mises equivalent stress, this radial stress acts as the third principal stress component, which, although often neglected in thin-walled cylinder assumptions because its value is much smaller than the circumferential and longitudinal stresses, still theoretically affects the Von Mises calculation through the combination of the three principal stresses $(\sigma\theta, \sigma z, \sigma r)$ so that in more accurate analyses, especially near the plastic limit or in thick-walled cylinders, radial stress contributes to lowering or raising the Von Mises stress value depending on its magnitude and distribution relative to the dominant tensile stress. This stress is usually smaller, with a negative sign indicating that the stress acts towards the inside of the tube.

c. Axial stress (σz)

This stress acts along the axis of the tube. Typically, the axial stress will be smaller than the circumferential stress and can be calculated using the following formula if there is an axial load, see Eq. (3).

$$\sigma z = \frac{pr}{2t} \tag{3}$$

Eq. (3) expresses the longitudinal stress that arises in the wall of a thin-walled cylinder due to internal pressure (p), where fluid pressure generates a force that tries to push the two ends of the cylinder apart so that the wall experiences tensile stress along the cylinder axis, with the magnitude of the stress being proportional to the pressure and the radius of the cylinder (r) and inversely proportional to the wall thickness (t); compared to the circumferential stress, the value of this longitudinal stress is only half because the cross-sectional area supporting the force is larger, but in relation to the Von Mises equivalent stress, the longitudinal stress still acts as the second main stress component that cannot be ignored, because the Von Mises criterion combines the interaction between circumferential stress and longitudinal stress through the relationship $\sigma vm = \sqrt{\sigma_\theta^2 - \sigma\theta\sigma z + \sigma_z^2}$ so that the presence of tensile stress increases the Von Mises stress value and directly affects the evaluation of the melting condition of materials in pipes or pressure vessels operating under internal pressure.

2.2.2 Von Mises stress

Von Mises stress is a failure criterion that combines normal stress and shear stress acting on a point in a material [11]. Von Mises stress can be calculated using an equation that takes into account circumferential, radial, and axial stresses, as in Eq. (4) [12]. The σvM equation describes tensile stress or stress in a coordinate system that uses the notation σ to represent stress components.

$$\sigma vm = \sqrt{\frac{1}{2}[(\sigma\theta - \sigma r)^2 + (\sigma r - \sigma z)^2 + (\sigma z - \sigma\theta)^2]} \quad (4)$$

where, σvM is the stress calculated in the average form or considered representing the principal stress in the system used. σθ is the stress in the θ direction, σr is the stress in the r direction, which is the radial direction from the center point or coordinate system. σz is the stress in the z direction, the vertical direction in stress analysis. In a hydraulic cylinder tube that only receives internal pressure (without axial load), it can be simplified by ignoring the axial stress (σz=0), as in Eq. (5).

$$\sigma vm = \sqrt{\frac{1}{2}[(\sigma\theta - \sigma r)^2 + (\sigma r)^2 + (\sigma\theta)^2]} \quad (5)$$

where σvM is the Von Mises stress calculated based on the existing stress components. Von Mises stress is often used in material failure criteria to determine when a material will undergo plastic deformation or failure. σθ is the stress acting in the tangential or angular direction (θ) on the material, which is often related to the circular direction in polar or cylindrical coordinate systems. σr is the radial stress acting in the radial direction on the material, usually pointing from the center outward (or vice versa) in radial coordinate systems. σθ is the stress component acting in other angular or tangential directions, which is the same as the σθ component.

2.3 Equation for tubes with internal pressure

If the circumferential stress (σθ) and radial stress (σr) are inserted into the Von Mises stress formula, the relationship between Von Mises stress and internal pressure in the tube is as shown in Eq. (6).

$$\sigma vm = \sqrt{\frac{1}{2}\left[\left(\frac{pr}{t} - \left(-\frac{pr^2}{t^2}\right)^2 + \left(-\frac{pr^2}{t^2}\right)^2 + \left(\frac{pr}{t}\right)^2\right)\right]} \quad (6)$$

where, σvM is the Von Mises stress calculated based on the difference in stress components in the analyzed system. Von Mises stress is used to determine material failure conditions based on a combination of normal and shear stresses. p is the pressure acting on the system or material being tested. r is the radius or other relevant measurement in the analysis system, which can be a radius or a specific distance. t is the thickness of the material or component being tested in the system.

Although there has been a lot of research related to hydraulic construction, there has been no research related to hydraulic performance based on the materials used, mainly due to the lack of comparative studies involving various materials under varying operational loads. Some researchers often focus only on material properties separately or do not consider all relevant load conditions. In addition, most studies have not extensively integrated multi-physics simulations, which can provide a more holistic understanding of material behavior in real conditions.

The objective of this study is to evaluate the performance of materials in piston cylinder designs used in military vehicle hydraulic actuators through experiments and FEA. This will provide scientific recommendations for material selection and minimize the risk of structural failure.

3 Method

This study combines experimental and numerical simulation methods to analyze material performance in the design of piston cylinder chambers for military vehicle hydraulic actuators.

3.1 Experimental

Experimental testing can validate the results of FEA and provide actual data for Von Mises stress and displacement. The experimental setup can be seen in Fig. 2.

Fig. 2 shows the experimental setup, illustrating the mechanical testing system used to measure the response of materials to applied loads. First, the load is applied to the specimen being tested. This load is usually applied using a hydraulic or mechanical system. Next, the load cell functions to measure the magnitude of the force or load applied to the specimen.

When the load is applied, the load cell converts the mechanical force into an electrical signal that can be processed by the measurement system. This signal provides accurate data on the magnitude of the load received by the specimen. Meanwhile, the piston rod is part of the hydraulic system that transfers pressure from the source to the specimen being tested. The piston moves according to the change in pressure applied, allowing the experiment to be applied evenly and in a controlled manner to the specimen.

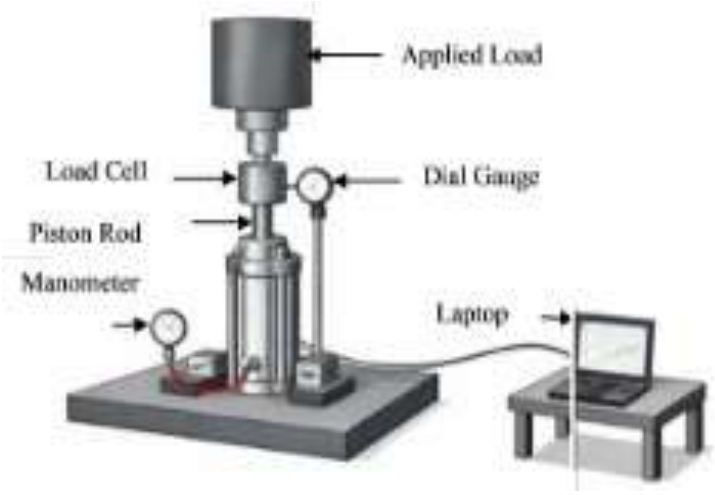

Fig. 2. Experimental setup

A dial gauge is used to measure changes in the shape of the specimen due to the application of load. When the load is applied, the specimen will deform, and the dial gauge will provide an accurate reading of how much deformation has occurred in the material. A manometer is used to measure the pressure in the hydraulic system that controls the application of the load. This ensures that the pressure applied to the specimen remains within the desired limits for the experiment. A laptop is used to monitor and acquire data from the load cell and analyze the data obtained during the experiment. The data collected from the load cell is forwarded to the laptop for further analysis.

The testing procedure begins with the application of an initial load of 450 N to the component and the measurement of displacement using a dial gauge and pressure data recorded on a manometer. Next, loads of 900 N and 1350 N are applied gradually, while recording changes in stress and displacement values at each load step. This test was conducted on several materials, namely AISI 1020, AISI 1035, and AISI A2 Tool Steel. The pressure and displacement results of each material were compared to evaluate the differences in performance of various materials in response to the applied load.

3.2 Simulation

This simulation uses FEA to model and analyze the mechanical behavior of materials under varying loads. The hydraulic actuator model was designed using SolidWorks® 3D and engineering parameters. The simulation was performed on three load variations: 450 N, 900 N, and 1350 N, and materials AISI 1020, AISI 1035, and AISI A2 Tool Steel.

The process began with model design using SolidWorks®, including the piston chamber as the main component. Finite element modeling was performed with a solid mesh for greater accuracy. FEA simulation was used to simulate the distribution of Von Mises stress and displacement in each material under the specified loads. During the simulation, the monitored parameters included Von Mises stress and maximum displacement. Von Mises stress was used to evaluate stress concentration, while displacement assessed

material deformation. Table 1 shows the mechanical properties of the test materials.

Table 1. Mechanical properties of AISI 1020, AISI A2 Tool Steel, and AISI 1035

Mechanical properties	AISI 1020	AISI A2 Tool Steel	AISI 1035
Modulus of elasticity	200000000 N/m²	203000 N/m²	204999.998 N/m²
Poisson's ratio	0.29 N/m²	0.285 N/m²	0.29 N/m²
Shear modulus	77000000 N/m²	79000 MPa	77500 MPa
Mass density	7900 kg/m³	7860 kg/m³	7849.9987 kg/m³
Tensile strength	420507000 N/m²	1860 - 2070	585.00029 N/m²
Compressive strength	415 MPa	2500 MPa	310 - 480 MPa
Melting strength	351571000 N/m²	-	-
Yield strength	-	1520 - 1720 Mpa	282.685049 N/m²
Thermal expansion coefficient	0.000015 K	1.1×10^{-5} K	1.1×10^{-5} K
Thermal conductivity	47 W/(m·°K)	20.0-24.0 W/m·°K	49.8-52.0 W/m·°K
Heat capacity	420 J/(kg·°K)	460	470 - 486 J/kg·°K
Material damping ratio	0.0001	60 - 62	0.85

The simulation process was carried out in several stages, beginning with the creation of a 3D model, followed by the determination of simulation parameters based on predetermined variables. The simulation was conducted with consideration given to the geometric configuration and the direction of the applied pressure.

Fig. 3 shows the creation of a network using adaptive structural connection elements, which aim to improve the accuracy of simulation results and stress evaluation. The parameters used in the simulation are listed in Table 2.

Load distribution is then applied to the critical interfaces of the components to create a simulation that reflects real-world conditions. This includes points that have high stress potential and greater loads, such as the connections between components and surface areas exposed to hydraulic pressure.

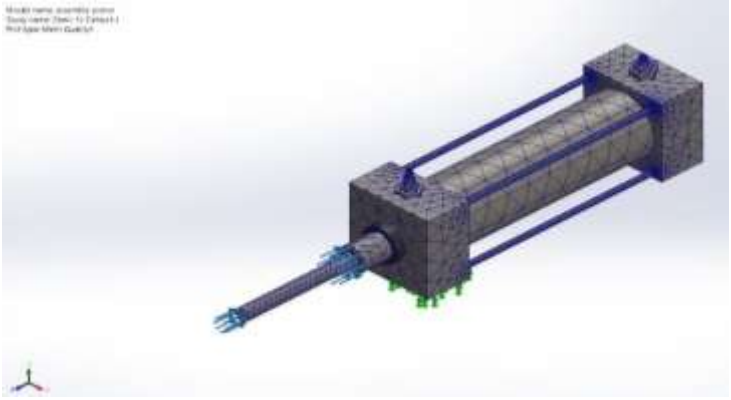

Fig. 3. Network modeling

Table 2. Mesh and boundary condition settings for FEA

Item	Description	Value
Analysis type	Structural FEA	Static simulation
Geometry	actuator cylinder component	Main component focus: piston chamber
Mesh type	Meshing method	Managed Program (Dense Network)
Meshing note	Element representation	Uses solid mesh for better accuracy
Material set	Materials compared	AISI 1020, AISI 1035, AISI A2 Tool Steel
Load cases	Loading variations	450 N, 900 N, 1350 N
Loading direction	Load/pressure direction	The simulation considers the geometry configuration and the direction of the applied pressure
Load application area	Load location/application region	Load distribution is applied at critical interfaces, including connections between components and surface areas exposed to hydraulic pressure
Boundary constraints	Supports/fixation	only mentions loading at critical interfaces/surfaces
Output parameters	Output metrics	Von Mises stress and maximum displacement

4 Results and discussion

4.1 Experimental results

The experiment yielded the results shown in Table 3. The results of the experiment in Table 3 show differences in Von Mises stress and displacement values for various loads and materials used in hydraulic actuators. There is an increase in Von Mises stress and displacement values as the applied load increases

Table 3. Effect of material and load on Von Mises stress and displacement

Load	Von Mises Stress (N/m²)			Displacement (cm)		
	AISI 1020	AISI 1035	AISI A2	AISI 1020	AISI 1035	AISI A2
450	52000	54000	60000	0.82	0.6	0.3
900	68000	79000	98000	1.0	0.85	0.65
1350	76000	93000	111000	1.5	1.2	0.95

4.2 Simulation results

The simulation results show the structure of components with different materials and load variations, namely AISI 1020, AISI 1035, and AISI A2 tool steel. The simulation produced the structural behavior of the equipment analyzed under various load conditions, namely 450 N, 900 N, and 1350 N. This section presents key performance indicators such as Von Mises stress and displacement. The simulation results are shown in Fig. 4 to Fig. 6.

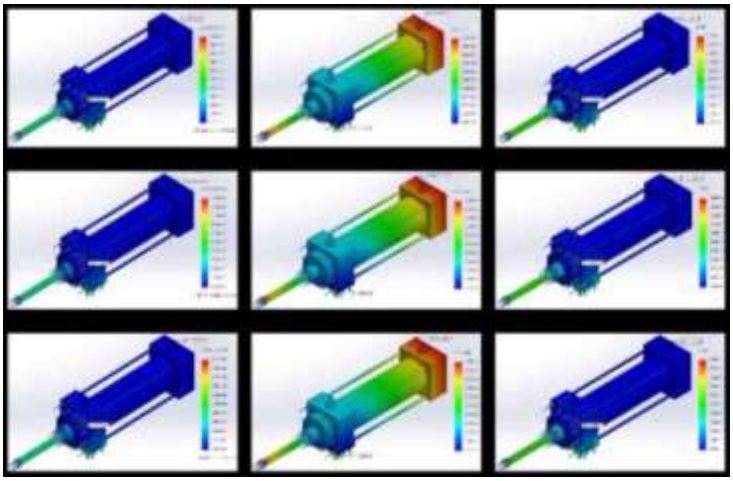

Fig. 4. Visualization of AISI 2020-cylinder simulation

Fig. 4 shows the results of a static simulation on an AISI 1020 drive cylinder. A maximum stress of 285 MPa was identified, concentrated in the bolt assembly and filler cap areas, although it was still below the material's melting point. The simulation revealed a maximum displacement of 0.82 mm on the piston axis, which could potentially affect hydraulic performance, as well as the highest local strain of 0.0045 mm/mm on the cylinder housing fillet radius, which could trigger fatigue cracks due to cyclic loading [13]. Three critical areas were identified, namely the bolt-filler cap interface, the sealing groove, and the piston rod transition. The safety factor of 1.23 obtained does not meet ASME standards, indicating the need for design optimization. In this study, the safety-factor interpretation refers to the ASME Boiler and Pressure Vessel Code (BPVC), Section VIII, Division 2, where the structural acceptance is evaluated using equivalent (Von Mises) stress against the allowable stress limits. Therefore, the reported safety factor is defined relative to the

allowable-stress criterion adopted from this ASME BPVC framework. Three critical areas were identified, namely the bolt-filler cap interface, the sealing groove, and the piston rod transition. The safety factor of 1.23 obtained does not meet ASME standards, indicating the need for design optimization or consideration of alternative materials for repetitive applications [14]. Fig. 5 shows the simulation results with AISI 1035 material.

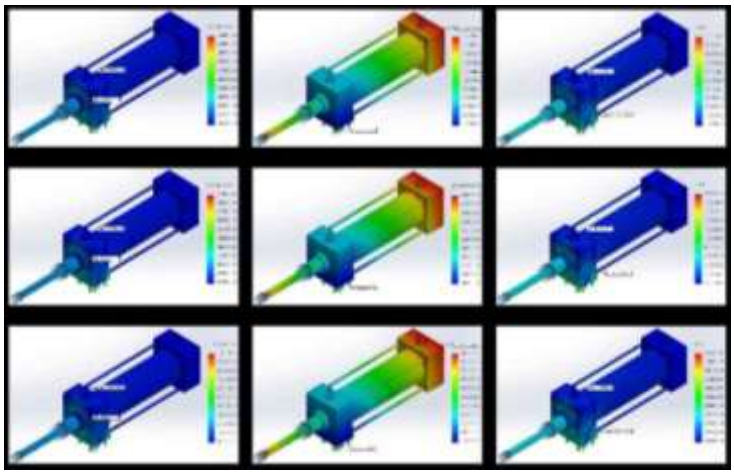

Fig. 5. Simulation visualization of AISI 1035 cylinder

Fig. 5 shows the simulation results of a drive cylinder made of AISI 1035 material, indicating a maximum Von Mises stress distribution of 324 MPa, concentrated in the bolt assembly area, and remaining within the material's yield strength limit of 460 MPa. The deformation pattern shows a maximum displacement of 0.65 mm, with the highest concentration occurring at the hydraulic seal interface, while local strain reaches 0.0038 mm in the fillet radius area of the cylinder housing. The analysis identified three critical areas showing the highest combination of mechanical parameters. The safety factor obtained was 1.42, showing a significant improvement over AISI 1020, although further geometric optimization is still needed to meet industrial pressure tank standards [15]. The more uniform stress distribution indicates better load redistribution characteristics in AISI 1035, with more evenly distributed stress concentrations along the body. These findings support the consideration of AISI 1035 as an optimal alternative material for drive cylinder applications operating under moderate to high pressure conditions [16].

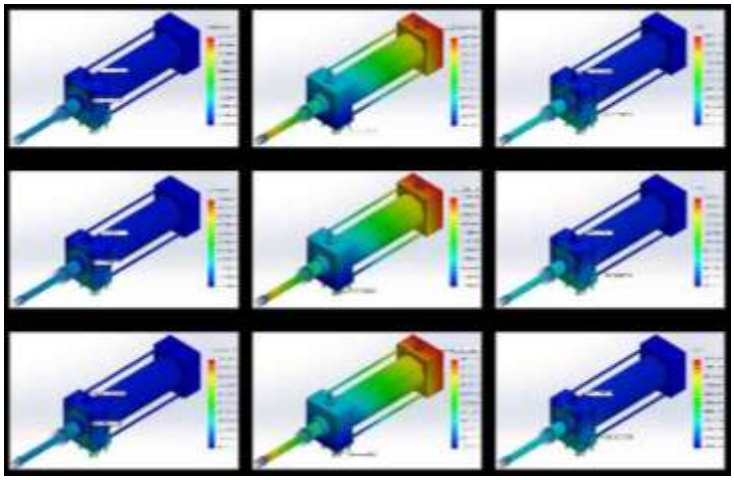

Fig. 6. Visualization of AISI A2 tool steel cylinder simulation

Fig. 6 shows the results of a static simulation of a drive cylinder made of AISI A2 tool steel. The analysis shows significantly superior mechanical performance compared to the previously tested materials. The maximum Von Mises stress recorded was 380 MPa, with the main concentration located in the bolt assembly thread area, well above the material's melting point of 1500 MPa. The simulation shows a highly controlled displacement of 0.28 mm, indicating optimal structural rigidity for precision applications. The maximum strain value only reaches 0.0018 mm/mm, distributed evenly along the fillet radius without significant local concentration. The safety factor reaches 3.94, far exceeding the ASME minimum requirements, with homogeneous stress distribution throughout the body [17]. The symmetrical deformation pattern and minimal local strain confirm excellent fatigue resistance under cyclic loading conditions. These results confirm the suitability of AISI A2 Tool Steel as a premium material for drive cylinder applications operating under extremely high pressures and continuous duty cycles [18]. A comparative evaluation of three load variations and three material types for drive cylinders is presented in Fig. 7.

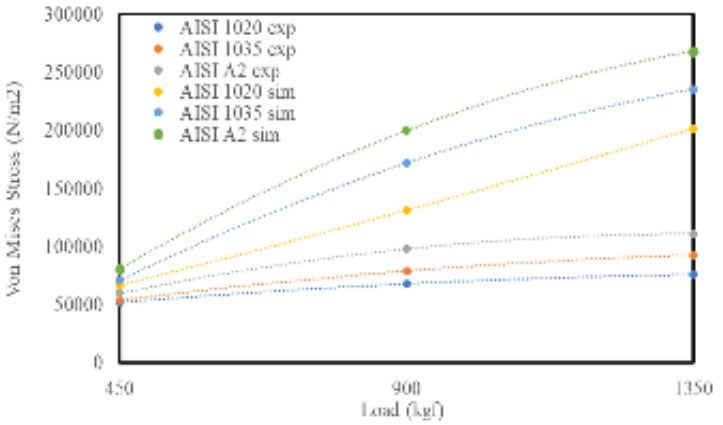

Fig. 7. Relationship between load and on Mises stress

Fig. 7 shows a clear relationship between Von Mises stress and applied load, where stress increases proportionally with increasing load on the actuator. For all tested materials, experimental results show a trend nearly identical to simulation results, confirming the consistency of the predictive model. Specifically, AISI 1035 showed the highest Von Mises stress at each load level, followed by AISI 1020 and AISI A2. This finding indicates that AISI 1035 is more susceptible to plastic deformation under load than other materials.

However, there were noticeable differences between the experimental and simulation results, with the experimental values being slightly lower than the simulation results for all materials. This may be due to variations in experimental conditions, such as material inhomogeneity or environmental factors that were not accommodated in the simulation. Despite these differences, the general trend of increasing stress with load remains consistent, confirming the reliability of the simulation in predicting material behavior under hydraulic load conditions. Von Mises stress analysis under various load conditions supports existing theories regarding material deformation and stress analysis, particularly the linear increase in Von Mises stress with increasing load. A comparison of materials shows that AISI 1035, due to its composition and microstructure, is more susceptible to higher stress levels under the same load conditions compared to AISI 1020 and AISI A2. This study is consistent with previous research, which also found a direct correlation between stress increase and applied load in similar material settings [19].

The experimental results are in line with previous findings on the importance of accurate stress prediction in hydraulic actuator design. Research on the need for careful material selection in actuator design, as different materials exhibit varying levels of stress tolerance, which directly affects the performance and durability of the actuator [20]. This study contributes to the field by presenting a detailed comparison between experimental results and simulated Von Mises stress values for materials commonly used in hydraulic actuator systems, namely AISI 1020, AISI 1035, and AISI A2. The differences between the experimental and simulated results are shown in Fig. 8.

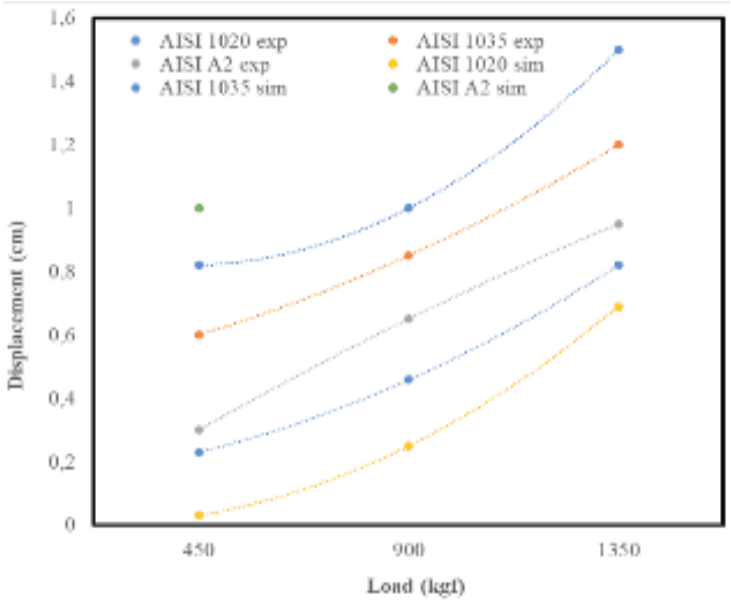

Fig. 8. Relationship between load and Von Mises stress

Fig. 8 shows the relationship between the applied load and the mechanical response of three materials: AISI 1020, AISI 1035, and AISI A2 obtained from experimental testing and finite element simulation. The response is represented by displacement, which correlates directly with the distribution of equivalent Von Mises stress under increasing load. In general, both experimental and numerical results exhibit a consistent monotonic increase as the load rises from 450 N to 900 N and 1350 N, indicating that the materials experience progressive stress–strain development with increasing external force. To quantify the deviation between the experimental and simulation results, the percentage difference was computed using |Sim−Exp|/Exp×100% for each material at each load level. For AISI 1020, the deviations were 52.80% (450 N), 33.89% (900 N), and 19.23% (1350 N); for AISI 1035, 61.78%, 46.08%, and 31.60%; and for AISI A2, 90.07%, 61.60%, and 27.44%, respectively. Overall, the discrepancy ranges from 19.23% to 90.07%, with an average absolute percentage difference of approximately 47.17%, confirming that the simulation systematically underpredicts the experimental response, particularly at lower loads. This systematic deviation is attributed to idealizations in the FE model, such as perfectly rigid boundary constraints, simplified contact/friction behavior, and the use of nominal material properties. Whereas the experimental measurements inherently include fixture and machine compliance, potential misalignment, and real material heterogeneity, which collectively increase the measured deformation.

Experimentally, AISI 1020 shows the highest response, increasing from 0.82 cm at 450 N to 1.00 cm at 900 N and reaching 1.50 cm at 1350 N. AISI 1035 demonstrates intermediate behavior, with values of 0.60 cm, 0.85 cm, and 1.20 cm at the same load levels, while AISI A2 exhibits the lowest displacement, rising from 0.30 cm to 0.65 cm and finally 0.95 cm. This ordering reflects the relative stiffness of the materials, where the lower carbon content of AISI 1020 results in lower yield strength and greater deformability, whereas AISI A2, as an alloyed tool steel, provides higher resistance to deformation.

The simulation results reproduce the same trend but with smaller absolute magnitudes. For AISI 1020, the predicted values increase from 0.0387 cm to 0.06611 cm and 0.2116 cm; for AISI 1035, from 0.02293 cm to 0.04583 cm and 0.1208 cm; and for AISI A2, from 0.00298 cm to 0.01496 cm and 0.06893 cm. The similarity in curve shape confirms that the finite element model successfully captures the mechanical behavior and the relative sensitivity of each material to loading, thereby providing good qualitative validation of the numerical approach.

The quantitative discrepancy between experimental and simulated values can be attributed to modeling idealizations. The numerical model typically assumes perfectly rigid boundary conditions, homogeneous and isotropic material properties, and nominal mechanical parameters taken from literature, while the real experiment includes additional compliance from fixtures, testing machine deformation, contact imperfections, and possible microstructural variations caused by manufacturing or heat treatment. These factors increase the measured deformation in experiments and are not fully represented in the simulation environment. Furthermore, frictional effects and slight misalignments during testing can amplify local stress redistribution, leading to higher equivalent Von Mises responses.

In addition, Fig. 7 shows that material displacement increases with increasing load on the hydraulic actuator, which is consistent with the theory of material mechanics that states that materials will experience greater deformation at higher loads. AISI 1020, which is low-carbon steel, shows greater displacement than AISI 1035 and AISI A2 at all load levels. This indicates that AISI 1020 is more elastic and more susceptible to elastic deformation at higher loads. Conversely, AISI A2, which is an alloy steel, exhibits better resistance to plastic deformation, resulting in less displacement under the same conditions.

These findings are also consistent with previous research, which shows that increased loads cause increased displacement in materials with higher elasticity. Smith et al. (2018) showed that more elastic materials, such as AISI 1020, deform more easily than harder materials, such as AISI A2. Low-carbon steels such as AISI 1020 are more elastic and exhibit greater deformation under increasing loads [21]. Meanwhile, AISI 1035, which has a higher carbon content, performs better than AISI 1020 but is still more susceptible to deformation than AISI A2.

This study makes a new contribution by comparing experimental and simulation results for three types of materials (AISI 1020, AISI 1035, and AISI A2) in the context of hydraulic actuators, providing a deeper understanding of how materials react to applied loads. In addition, this study also provides new insights into the differences between experiments and simulations in predicting material displacement, which has rarely been discussed in depth in previous literature.

Several previous studies have examined the effect of load on material deformation, but not many have discussed the comparison between experiments and simulations in detail for the same material, especially in hydraulic actuator applications. Materials with low carbon content, such as AISI 1020, show greater deformation [22], which is in line with the findings of this study. Meanwhile, high-carbon steel, such as AISI 1035, experiences less deformation than low-carbon steel [23], but more than alloy steel, such as AISI A2.

This study is limited to static loading conditions and assumes idealized boundary conditions and material behavior in the numerical model. Effects such as cyclic (fatigue) loading, thermal influences, and potential experimental-system compliance were not considered and should be addressed in future work to obtain a more comprehensive evaluation of structural performance.

5 Conclusion

This study provides a comparative structural assessment of AISI 1020, AISI 1035, and AISI A2 steels for hydraulic actuator cylinder applications under static loading conditions. The FEA and experimental results show that AISI 1020 experiences the largest displacement and lowest safety factor, indicating limited suitability for high-load conditions. AISI 1035 demonstrates improved performance compared to AISI 1020 but remains inferior to AISI A2. Among the evaluated materials, AISI A2 exhibits the smallest displacement and highest safety factor, confirming superior resistance to deformation and stress concentration. These emphasize the importance of material mechanical strength and stiffness in actuator structural reliability. FEA proved to be an effective tool for predicting stress distribution and supporting material selection decisions. Future work will extend this study to include fatigue loading and thermo-mechanical effects, allowing evaluation of

material performance under cyclic stresses and temperature variations that more closely represent actual operating conditions.

References

[1] V. Claps, C. Bachmann, G. Janeschitz, and R. Mozzillo, "Conceptual design of DEMO breeding blanket in-vessel toroidal transporter," Fusion Eng. Des., vol. 202, no. October 2023, p. 114389, 2024, doi: 10.1016/j.fusengdes.2024.114389.

[2] Y. Xu et al., "Experimental analysis of the multiaxial failure stress locus of commercially pure titanium at low and high rates of strain," Int. J. Impact Eng., vol. 170, no. January, p. 104341, 2022, doi: 10.1016/j.ijimpeng.2022.104341.

[3] L. Pagliari, F. Concli, R. Gandhi, and M. Salmi, "Multiaxial fatigue behavior of triply periodic minimal surface lattice structures in Ti6Al4V fabricated by laser powder bed fusion under combined axial – torsional loading," vol. 38, no. April, pp. 3655–3671, 2025, doi: 10.1016/j.jmrt.2025.08.152.

[4] S. Kumar, P. Arora, S. K. Gupta, and J. Chattopadhyay, "Novel Test Methodology for Peak Strain-Controlled Notched Fatigue Test," Procedia Struct. Integr., vol. 71, pp. 34–41, 2025, doi: 10.1016/j.prostr.2025.08.006.

[5] Z. Lu and B. Wu, "Numerical Analysis of a Novel Prefabricated Concrete Beam with Double-Grouted Couplers under Static Loading," KSCE J. Civ. Eng., vol. 27, no. 8, pp. 3501–3516, 2023, doi: 10.1007/s12205-023-0244-4.

[6] N. Karathanasopoulos and D. Mohr, "Strength and Failure of Self-Piercing Riveted Aluminum and Steel Sheet Joints : Multi-axial Experiments and Modeling," J. Adv. Join. Process., vol. 5, no. February, p. 100107, 2022, doi: 10.1016/j.jajp.2022.100107.

[7] V. Grolleau, C. C. Roth, and D. Mohr, "Design of in-plane torsion experiment to characterize anisotropic plasticity and fracture under simple shear," Int. J. Solids Struct., vol. 236–237, no. September 2021, p. 111341, 2022, doi: 10.1016/j.ijsolstr.2021.111341.

[8] N. Buratti, V. Pollini, and C. Mazzotti, "Experimental characterization of the mechanical behaviour of U-shaped dissipative devices," Procedia Struct. Integr., vol. 44, no. 2022, pp. 1196–1203, 2023, doi: 10.1016/j.prostr.2023.01.154.

[9] R. Shotri, T. Miura, P. Geng, Y. Morisada, and K. Ushioda, "Understanding thermal-mechanical variations and resulting joint integrity of pressure-controlled linear friction welding of thin-steel sheets," Int. J. Mach. Tools Manuf., vol. 204, no. November 2024, p. 104235, 2025, doi: 10.1016/j.ijmachtools.2024.104235.

[10] C. B. Niutta et al., "Very high cycle fatigue (VHCF) response of an Additively manufactured Nitinol ☆," Int. J. Fatigue, vol. 200, no. April, p. 109130, 2025, doi: 10.1016/j.ijfatigue.2025.109130.

[11] V. Widerspan, S. Shojai, and E. Ghafoori, "Enhanced local fatigue approach for welded tubular joints using 3D digital scans and implicit gradient model," vol. 199, no. April, 2025, doi: 10.1016/j.ijfatigue.2025.109060.

[12] F. Najafnia, H. Talebi-ghadikolaee, A. H. Bamdad, E. Dorchepour, and R. Hashemi, "Evaluation of constitutive modeling for dynamic plastic-fracture modeling of dual phase (DP590) steel sheets," J. Mater. Res. Technol., vol. 36, no. August 2024, pp. 10210–10221, 2025, doi: 10.1016/j.jmrt.2025.05.154.

[13] K. Lee, B. Cho, K. J. R. Rasmussen, and D. Jung, "Experimental and numerical investigation of bolt-free preloaded connection for steel-framed modular buildings," J. Constr. Steel Res., vol. 220, no. February, p. 108827, 2024, doi: 10.1016/j.jcsr.2024.108827.

[14] G. Bufalari, N. Troost, H. Den Besten, and M. L. Kaminski, "Mode- { I , III } multiaxial fatigue testing of high-quality welds in steel maritime structures using a hexapod," vol. 197, no. November 2024, 2025.

[15] M. S. Xavier, S. M. Harrison, D. Howard, Y. K. Yong, and A. J. Fleming, "International Journal of Mechanical Sciences Modeling of soft fluidic actuators using fluid – structure interaction simulations with underwater applications," vol. 255, no. May, 2023.

[16] D. Obkircher, M. Costas, M. Langseth, and A. H. Clausen, "Quasi-static and dynamic shear-out resistance in a steel fin-plate connection : An experimental and numerical investigation," Int. J. Impact Eng., vol. 192, no. April, p. 105012, 2024, doi: 10.1016/j.ijimpeng.2024.105012.

[17] C. Widstrand, C. Hu, X. Mao, J. Labuz, and S. Gonella, "Stress focusing and damage protection in topological Maxwell metamaterials," Int. J. Solids Struct., vol. 274, no. April, p. 112268, 2023, doi: 10.1016/j.ijsolstr.2023.112268.

[18] S. Liu, Y. Gorash, M. Fotouhi, and D. Mulvihill, "Visually readable sensors for fatigue life monitoring of safety- critical structures," Procedia Struct. Integr., vol. 75, pp. 200–204, 2025, doi: 10.1016/j.prostr.2025.11.022.

[19] E. Zacchei, A. Tadeu, J. Almeida, M. Esteves, M. Inês, and S. Silva, "Materials & Design Design of new modular metal pallets : Experimental validation and life cycle analysis," Mater. Des., vol. 214, p. 110425, 2022, doi: 10.1016/j.matdes.2022.110425.

[20] Y. Nouri, H. Ghasemi, and A. Haghollahi, "Results in Engineering Experimental and numerical study of seismic performance and failure mechanisms of multi-story elliptic and Quasi-X braced resisting frames," Results Eng., vol. 26, no. April, p. 105657, 2025, doi: 10.1016/j.rineng.2025.105657.

[21] G. Veile et al., "Comparison of experimental and numerical fatigue life of austenitic stainless steel components at 300 ◦ C with idealized and scanned weld geometries," Int. J. Fatigue, vol. 195, no. February, p. 108873, 2025, doi: 10.1016/j.ijfatigue.2025.108873.

[22] B. Barsotti, C. Battini, M. Gaiotti, and C. Mario, "Experimental and numerical assessment of ultimate strength of a transversally loaded thin-walled deck structure," Mar. Struct., vol. 103, no. February, p. 103793, 2025, doi: 10.1016/j.marstruc.2025.103793.

[23] J. Magliaro and W. Altenhof, "Forces in Mechanics Conceptualization , proposed design and theoretical investigations of an active adaptive cutting device with enhanced energy dissipation potential," Forces Mech., vol. 9, no. July, p. 100122, 2022, doi: 10.1016/j.finmec.2022.100122.